VELOCITY STRUCTURE AND PROPERTIES OF THE LUNAR CRUST*

M. N. TOKSŐZ, F. PRESS, K. ANDERSON, and A. DAINTY
Dept. of Earth and Planetary Sciences, Massachusetts Institute of Technology, Cambridge, Mass., U.S.A.

G. LATHAM, M. EWING, J. DORMAN, D. LAMMLEIN, and Y. NAKAMURA
Lamont-Doherty Geological Observatory, Palisades, New York, U.S.A.

G. SUTTON, and F. DUENNEBIER
University of Hawaii, Honolulu, Hawaii, U.S.A.

Abstract. Lunar seismic data from three Apollo seismometers are interpreted to determine the structure of the Moon's interior to a depth of about 100 km. The travel times and amplitudes of *P* arrivals from Saturn IV B and LM impacts are interpreted in terms of a compressional velocity profile. The most outstanding feature of the model is that, in the Fra Mauro region of Oceanus Procellarum, the Moon has a 65 km thick layered crust. Other features of the model are: (i) rapid increase of velocity near the surface due to pressure effects on dry rocks, (ii) a discontinuity at a depth of about 25 km, (iii) near constant velocity (6.8 km/s) between 25 and 65 km deep, (iv) a major discontinuity at 65 km marking the base of the lunar crust, and (v) very high velocity (about 9 km/s) in the lunar mantle below the crust. Velocities in the upper layer of the crust match those of lunar basalts while those in the lower layer fall in the range of terrestrial gabbroic and anorthositic rocks.

1. Introduction

With the successful recording of Lunar Module (LM) ascent stage and upper stage of the Saturn rocket (S-IV B) impacts by the Apollo 12, 14, and 15 seismometers, discrete seismic phases which can be interpreted in terms of a velocity structure inside the Moon have become available. Travel times, amplitudes, and wave shapes of compressional (P) waves have been obtained for distances between $\Delta = 67$ km and $\Delta = 357$ km. These data can be inverted to determine the seismic velocity structure in the outer 100 km of the lunar interior. In this paper we briefly describe the data, the inversion techniques, velocity model, and compositional significance of the model in the light of laboratory measurements of velocities of lunar and terrestrial rocks.

In the study of the Earth's interior, seismic techniques have provided the most direct evidence for its structure, composition and properties. Data from a large number of earthquakes of all magnitudes, numerous artificial sources (*e.g.* underground nuclear explosions) and more than a thousand seismic stations have been utilized for these studies. In the case of the Moon the natural seismicity (both the number and energy of moonquakes) is many orders of magnitude lower than that of the Earth (Latham *et al.*, 1971a,b). With only three stations it is not possible at this stage to specify the epi-

* Lamant-Doherty Geological Observatory Contribution No. 1768.

Communication presented at the Conference on Lunar Geophysics, held between October 18–21, 1971, at the Lunar Science Institute in Houston, Texas, U.S.A.

center coordinates, focal depth, and origin time of these events with sufficient accuracy so that they could be used in structural studies. It has not been possible to detect long-period surface waves or free oscillations of the Moon from such very small moonquakes. Thus we must rely on six artificial impacts (of known location and origin time) for the study of the lunar interior. In the next section data from these impacts are discussed. The inversion techniques and the resultant velocity structure are described in Section 3. The compositional significance of the velocity model is covered in the final section.

2. Seismic Signals from Artificial Impacts

Signals from the impacts of S-IV B and LM-ascent stages have been recorded by three (Apollo 12, 14, and 15) seismometers. The locations of the three operating stations and the artificial impacts, relevant distances, and energies are listed in Table I. Locations and wave paths are also shown in Figure 1. In understanding Table I, it is important to keep in mind that the S-IV B impact precedes the lunar landing and thus

TABLE I

A. COORDINATES OF SEISMIC STATIONS AND IMPACT POINTS AND RELEVANT DISTANCES

Stations and impacts	Coordinates (degrees)	Distances (in km) from		
		Apollo 12 site	Apollo 14 site	Apollo 15 site
Apollo 12 Site	3.04 S, 23.42W	–	–	–
Apollo 14 Site	3.65 S, 17.48W	181	–	–
Apollo 15 Site	26.08N, 3.66E	1188	1095	
Apollo 12 LM Impact	3.94 S, 21.20W	73	–	–
Apollo 13 S-IV B Impact	2.75 S, 27.86W	135	–	–
Apollo 14 S-IV B Impact	8.00 S, 26.06W	170	–	–
Apollo 14 LM Impact	3.42 S, 19.67W	114	67	–
Apollo 15 S-IV B Impact	1.36 S, 11.77W	357	186	–
Apollo 15 LM Impact	26.36N, 0.25E	1130	1049	93

B. IMPACT PARAMETERS

Impact	Date day-month-yr	Time (hr:min:s)	Velocity (km/s)	Mass (kg)	Kinetic energy (ergs)	Angle from horizontal (degrees)
Apollo 12 LM	20-11-69	22:17:17.7	1.68	2383	3.36×10^{16}	3.7
Apollo 14 LM	7-02-71	00:45:25.7	1.68	2303	3.25×10^{16}	3.6
Apollo 15 LM	3-08-71	03:03:37.0	1.70	2385	3.44×10^{16}	3.2
Apollo 13 S-IV B	15-04-70	01:09:41.0	2.58	13925	4.63×10^{17}	76
Apollo 14 S-IV B	4-02-71	07:40:55.4	2.54	14016	5.54×10^{17}	69
Apollo 15 S-IV B	29-07-71	20:58:42.9	2.58	13852	4.61×10^{17}	62

is recorded by stations operating prior to the landing. The LM-ascent stage impact which occurs after the lunar landed mission is completed can be recorded with the instrument of the same mission. Furthermore, the kinetic energy of a typical S-IV B impact is about 13 times larger than that of a typical LM impact. First arrivals from

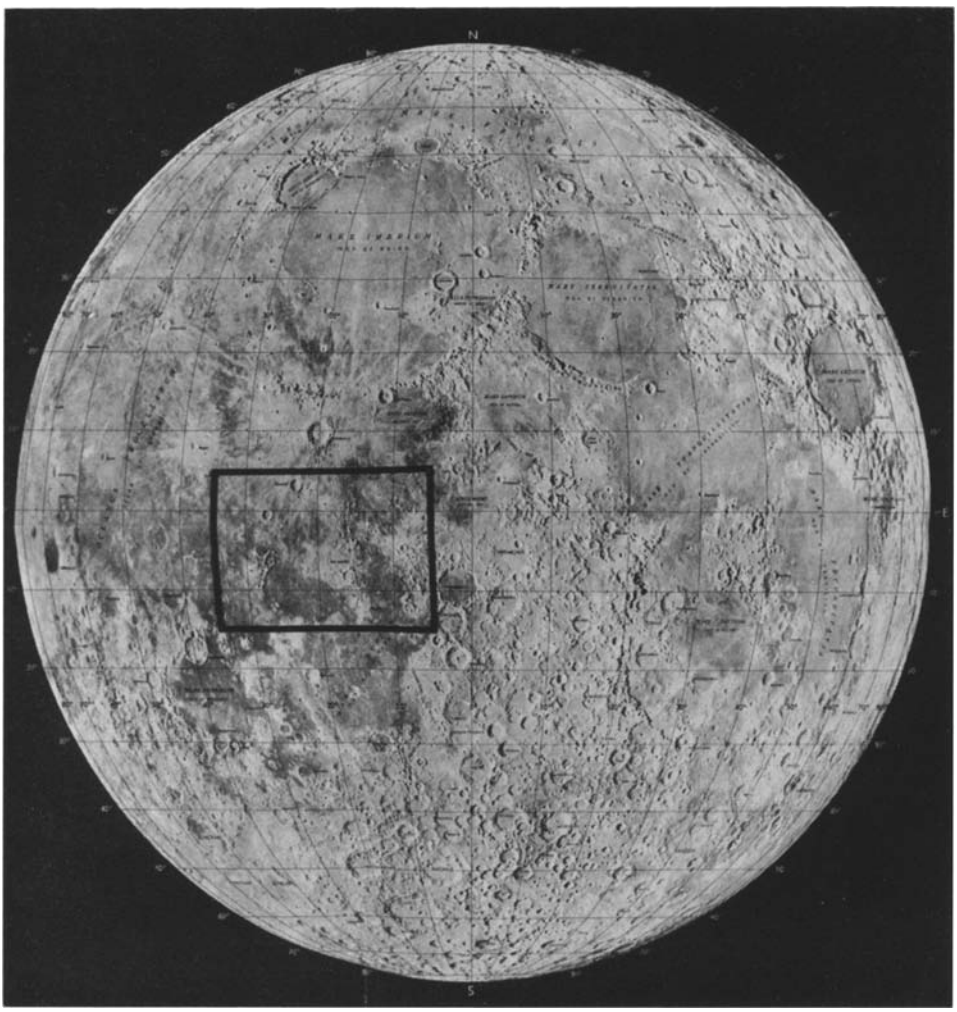

Fig. 1a. Location map showing the region (in frame) of the moon where most of the seismic observations have been made.

LM impact data have been usable to a distance of 114 km, while those of S-IV B impacts to the maximum available distance of 357 km.

The general characteristics of all impact signals are very similar to each other. They are extremely prolonged with gradual build-up of the signal and very long exponential decay of signal intensity. Typically, duration of the signals is about two hours. These characteristics, which are believed to be caused by intensive scattering, have been

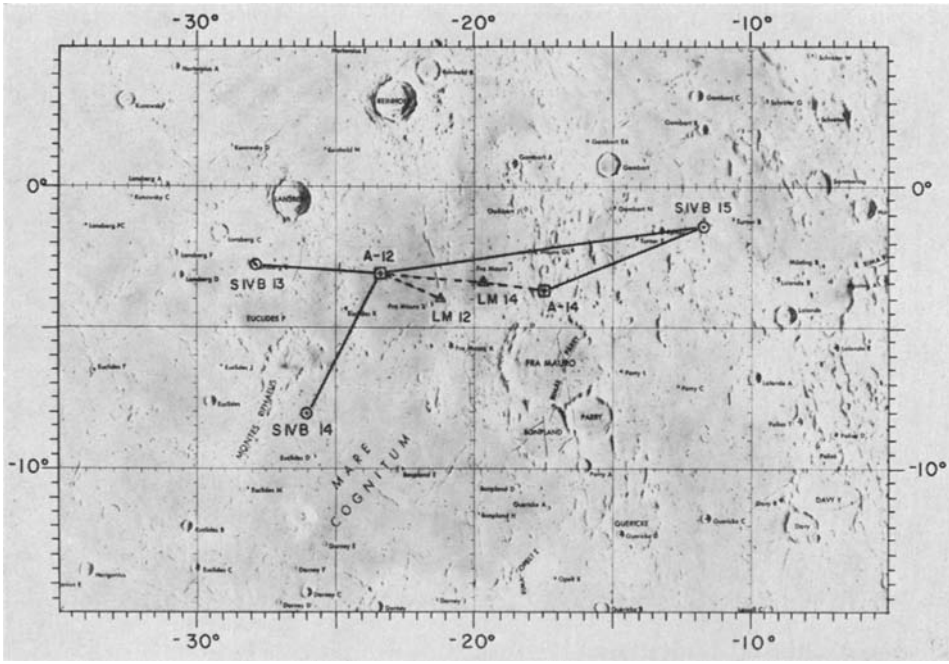

Fig. 1b. Enlarged picture illustrating Apollo 12 and 14 seismic stations, impact points and seismic ray paths.

discussed in a previous publication (Latham *et al.*, 1970) and will not be repeated here. The signals corresponding to the arrival of discrete seismic phases can be identified in the early parts of the records. These would be of most interest for our study.

The initial portions of the impact seismograms are shown in Figure 2. The larger amplitude and higher signal-to-noise ratio of S-IV B impact records relative to those of LM impacts are clearly illustrated. The change in the signal characteristics from one record to another, at different distances such as $\Delta = 135$, 172, and 357 km, is also observed. The travel times and amplitudes of P-wave arrivals, and the match of the general properties of seismograms (first and later arrivals) are utilized for the interpretation of the records in terms of a velocity structure.

The travel times of first arrivals provide the most direct means of looking at the lunar interior. The arrivals could be timed to an accuracy of about 0.2 s, where signal-to-noise ratio is high. In other cases uncertainties of 0.5 s or greater might be encountered. For timing the first arrivals and identifying later phases, multi-band filtered records are utilized. For *P*-waves times are read from high-pass filtered or unfiltered traces. Positive identification of the signal is made by the linear polarization of the particle motion. An example of three-component seismograms filtered at two separate pass-bands is shown in Figure 3. Note the P-wave stands out more clearly at vertical component high-pass filtered traces, while the S-waves and some later arrivals are clearer at lower frequency pass-band data.

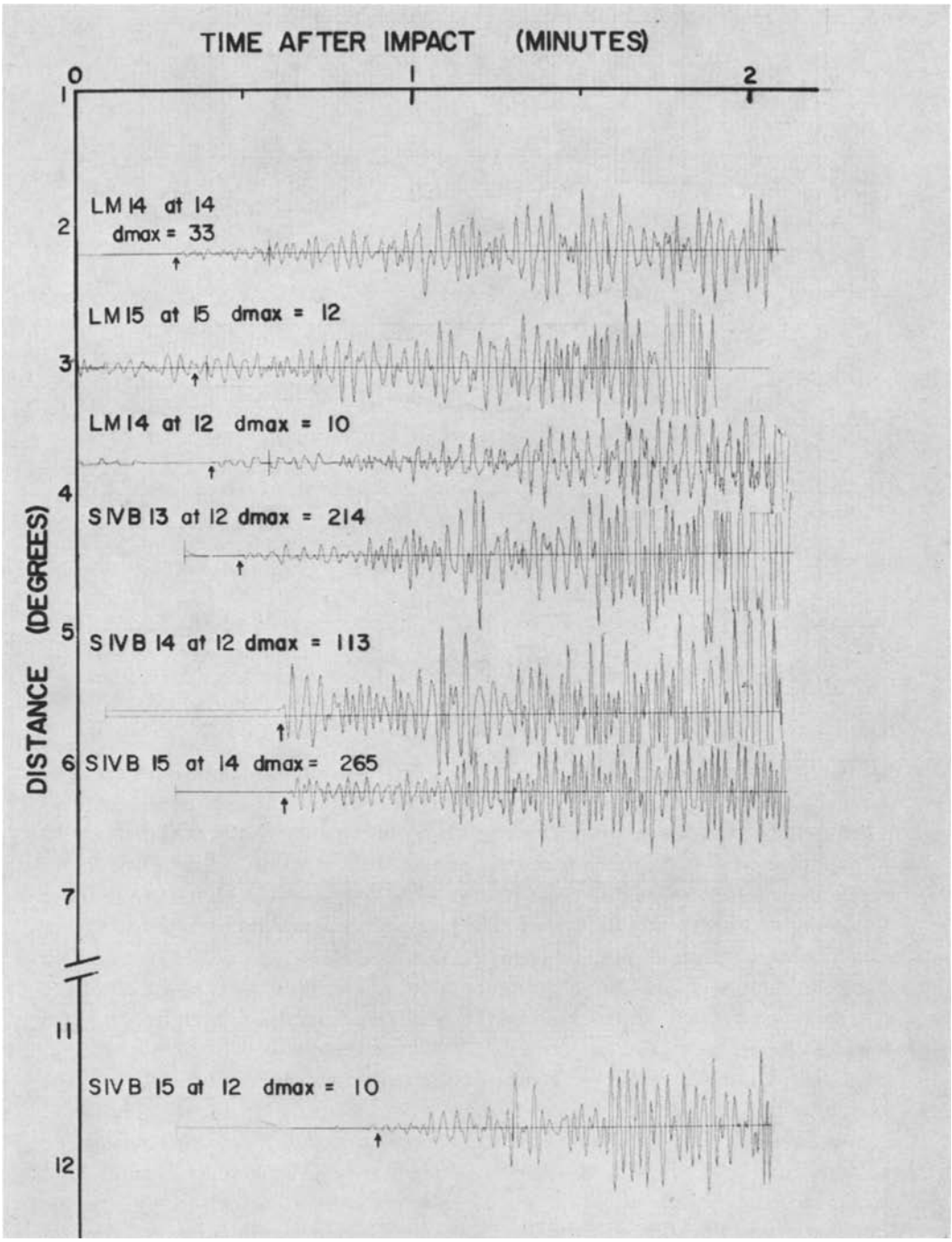

Fig. 2. A composite illustration of vertical components of seismograms recorded from all artificial impacts. Notation 'LM 14 at 14' means LM-14 impact recorded at Apollo 14 seismic station. 'dmax' is the amplitude normalization scale; to obtain true relative amplitudes, seismogram amplitudes must be multiplied by this factor. Distance is in degrees; 1 degree = 30.3 km. Arrows indicate the first arrival. Note the change of character of S-IV B seismograms with distance.

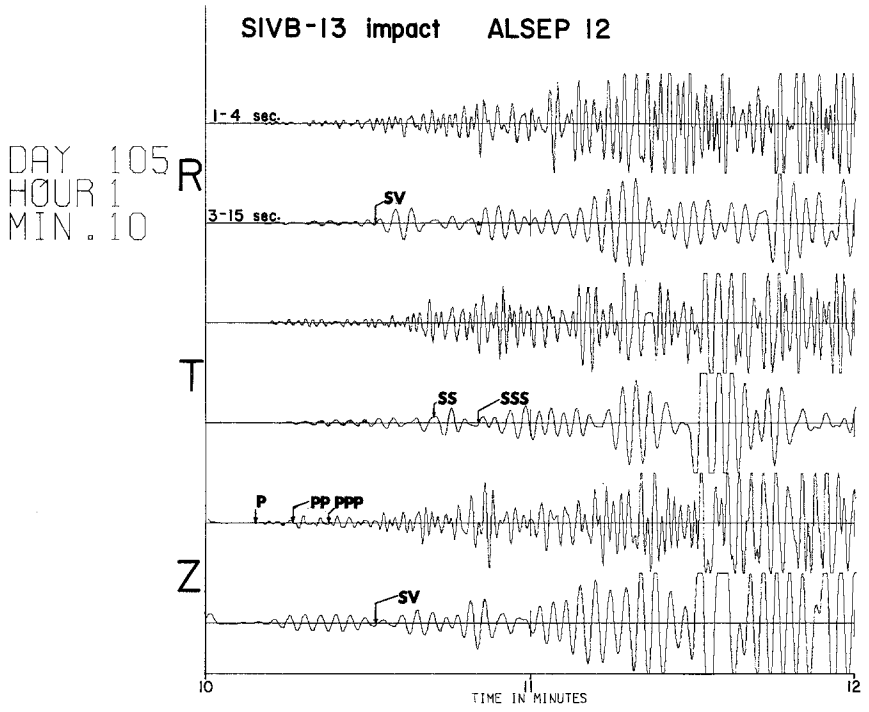

Fig. 3. Seismogram of Apollo 13 S-IV B impact recorded at the Apollo 12 station. *R*, *T*, and *Z* indicate radial, transverse, and vertical components of the motion, respectively. Each seismogram is band-pass filtered at two period intervals: 1-4 s and 3-15 s. P, PP, PPP, S and SS arrivals are shown.

The travel time-distance curve shown in Figure 4 is a composite of data for first arrival P-waves and later phases (surface-reflected PP, PPP). Since both source and receiver are at the surface of the Moon, for phases such as PP and PPP the times can be plotted at equivalent distance for first arrivals. The overall characteristics of the travel times indicate rapidly increasing velocities near the surface. An intermediate zone with nearly constant velocity and below this a high velocity zone are indicated by the two branches of the travel time curve between distances of 186 km and 357 km. In addition to these, later arrivals observed at 186 and 357 km indicate the presence of very high velocity gradients or discontinuities inside the moon.

The amplitudes (Figure 4) provide further evidence for velocity discontinuities. Because the geometric focusing, defocusing and reflection of seismic rays are controlled by the velocity gradients, the amplitudes are very sensitive indicators of rapid velocity variations. The data in Figure 4 come from both the LM and S-IV B impact records. Since the sources have different energies, the amplitudes need to be scaled. We chose an empirical approach for this purpose and required a smooth transition from LM signal amplitudes to S-IV B signal amplitudes as a function of distance. This required a correction (multiplication) factor of 20 for LM amplitudes, a value larger than the square-root of energy ratios. However, since the angles of impact (about 3° from

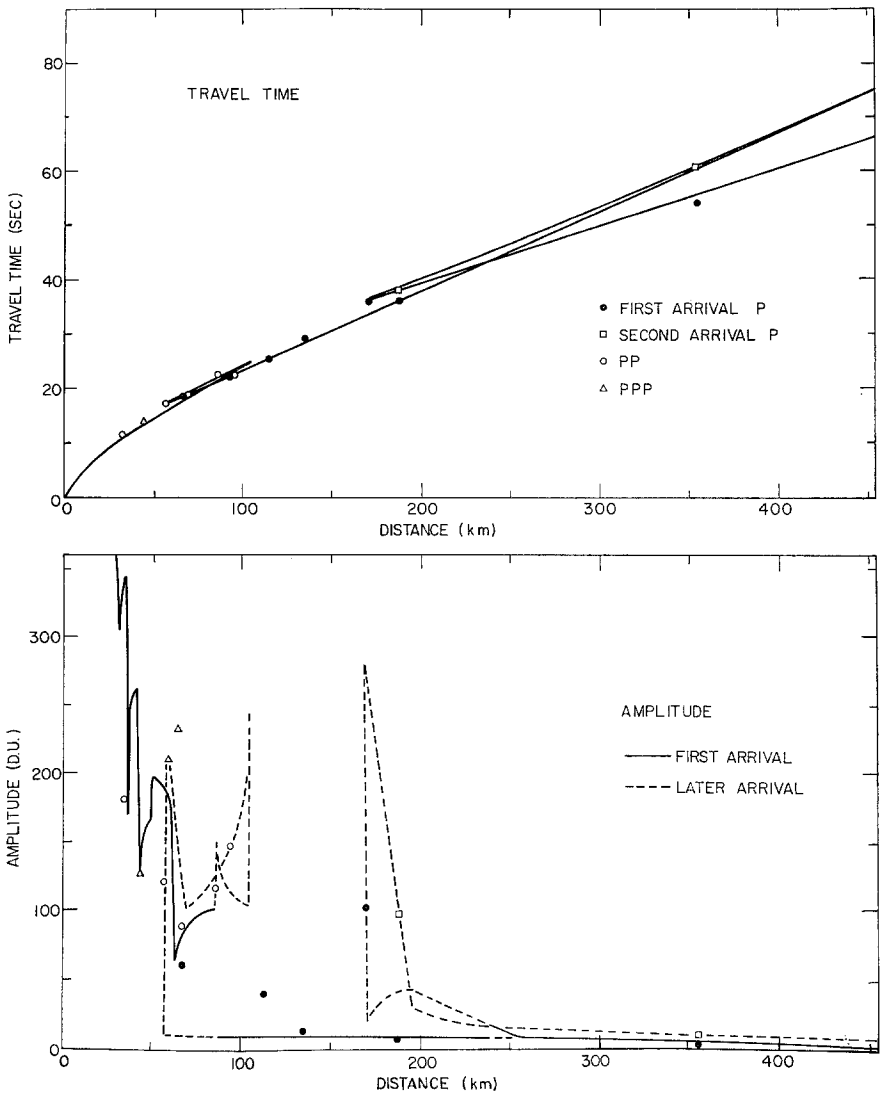

Fig. 4. Travel times and amplitudes of P-wave pulses. 'Second arrival' P denotes a relatively large amplitude pulse that arrives after P and which is associated with a travel time cusp. PP and PPP are surface reflected phases. Lines are theoretical curves for velocity model given in Figure 7. Note the large amplitudes associated with travel time cusps. 'D.U.' signifies digitization unit.

horizontal for LM vs 62° or greater for S-IV B) and sizes of the impacting objects were different, it is reasonable that S-IV B impacts would be more efficient generators of seismic waves at frequencies below 1 Hz.

The agreement between theoretical curves and observed amplitudes are good considering the experimental and theoretical limitations of the procedure. The effects of focusing, multiplicity of travel time curves, and caustics are illustrated in Figure 5

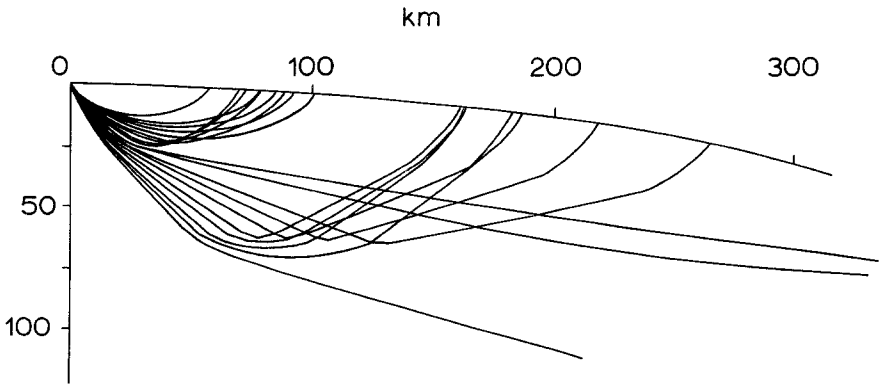

Fig. 5. Seismic ray paths inside the moon (velocity model is shown on left) for a surface source. Ray crossings correspond to multiplication of travel times. High density of rays indicates focusing of energy and hence large amplitudes.

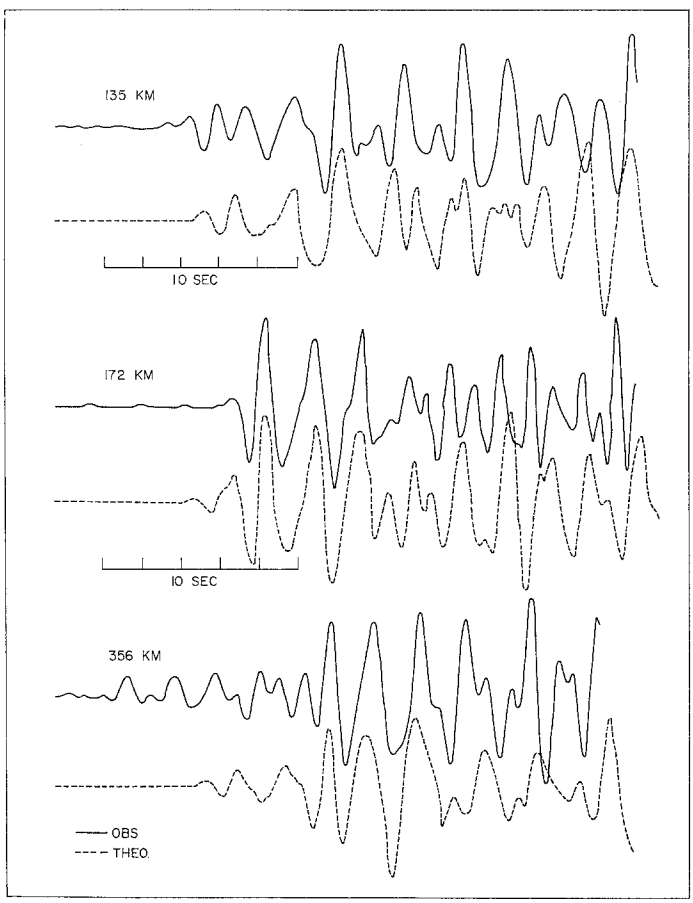

Fig. 6. Observed (solid line) and synthetic (dashed line) seismograms for three S-IV B impacts recorded at Station 12. The change in seismic pulse shapes and relative amplitudes of first and later arrivals with increasing distance is obvious. At 356 km the first two peaks of observed seismograms are noise pulses and can be clearly identified as such in unfiltered seismograms.

through ray tracing. The crossing rays result from high velocity gradients and discontinuities.

A more definitive approach to interpreting the observed lunar seismograms is to compute their theoretical equivalents. A practical approach to the theoretical seismograms as applied to body waves is to utilize modified Cagniard-de Hoop techniques with generalized rays as described by Helmberger (1968) and Helmberger and Wiggins (1971). This requires, in addition to the velocity structure inside the Moon, knowledge of the seismic source pulse due to the impact and the exact impulse response of the seismometer emplaced at the surface on a very low velocity regolith complex. To isolate the effect of the velocity structure we must determine the other variables. Fortunately the structure and especially the velocity gradients and discontinuities play the most important role in controlling many of the prevailing characteristics of the seismograms. Furthermore, it is possible to isolate the structural contribution by keeping other parameters (source and receiver responses) nearly constant. In this investigation we utilized this approach. We chose the three S-IV B impact seismograms recorded by the Apollo 12 station. This had the advantage of keeping the instrument response fixed while the source-receiver distance increased for three nearly identical impacts (Table I). Because of the low signal-to-noise ratios, LM impact seismograms were excluded from matching.

The observed and computed seismograms at distances of $\Delta = 135$, 172, and 357 km are shown in Figure 6. The source function was chosen such that at 172 km the seismograms were matched exactly for the first 10 s. The general characteristics of the observed seismograms change significantly from $\Delta = 135$ km to 172 km and again from $\Delta = 172$ km to 357 km. At the shortest distance the gradual increase in the amplitudes is apparent. At 172 km (also at $\Delta = 186$ km in Figure 2) the first arrival is the largest pulse in the wave train. At 357 km a small amplitude refracted arrival is followed 5 s later by a large amplitude wave. These features and the other general characteristics are matched very closely by the theoretical seismograms. The overall agreement between the observed and theoretical records are very good although there are some discrepancies. When dealing with a highly scattering body with surface heterogeneities, a multitude of seismic paths, and different sources, it is not realistic to expect a better fit to the data with a single structure and single source function.

The velocity model finalized on the basis of the fit to the travel times, amplitudes and synthetic seismograms is shown in Figure 7. The main features of the velocity profile are:

(i) Very rapid increase at very shallow depths from a surface value of 0.1 km/s (Kovach *et al.*, 1971) to about 5 km/s at 10 km depth.

(ii) A sharp increase ('discontinuity') at a depth of about 25 km.

(iii) Near constant value (about 7 km/s) between 25 and 65 km.

(iv) A significant and discontinuous increase at the base of the lunar crust (65 km).

(v) As can be determined from a single data point corresponding to the distance of 357 km, very high velocity (greater than 9 km/s) below the lunar crust.

The main features of the model, such as the 'discontinuities' at about 25 km and

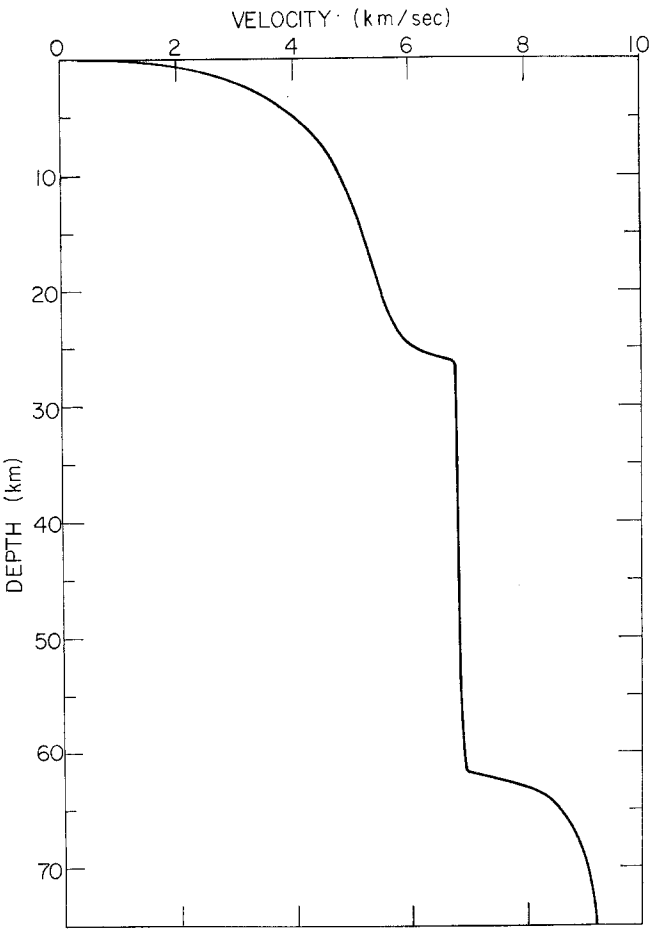

Fig. 7. Compressional velocity versus depth profile for the moon in the vicinity of Fra Mauro (see Figure 1b).

65 km depths, are supported not only by the amplitudes and travel times of the first arrivals, but also with the times and amplitudes of the later arrivals. When the available data are accepted, it is not possible to find suitable models without discontinuities. Some details of the model, such as the nature of increase of the velocities (whether it is a smooth or stepwise increase) in the upper 5 km, cannot be resolved without additional data at distances closer than 30 km. The physical and compositional significances of this velocity model are discussed in the next section.

3. Compositional Implications

The seismic velocity profile inside the Moon (Figure 7) provides direct evidence for the presence of a layered lunar crust. From comparisons with velocities of the Earth's crust and mantle, it is appropriate to define the base of the 'lunar crust' at the dis-

continuity at 65 km. Although this is greater than the average thickness of the Earth's crust, the jump of the velocity at this interface from about 7.0 to 9.0 km/s is very similar to the increase at the Mohorovičič discontinuity. If hydrostatic pressure instead of depth is used as the variable, the base of the lunar crust occurs at a pressure of 3.5 kb, which is reached at a depth of 10 km inside the Earth.

The compositional implications of the lunar velocity model can be explored with the aid of high-pressure laboratory measurements on lunar and terrestrial rocks. This is illustrated in Figure 8. Velocity measurements have been made on lunar soils,

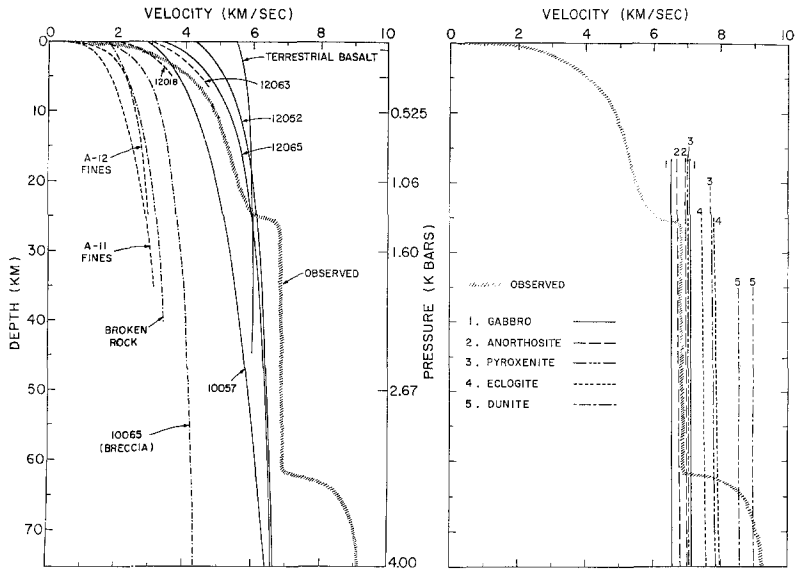

Fig. 8. Observed velocity profile and velocities of lunar and terrestrial rocks measured in the laboratory as a function of pressure. On the left, lunar rocks are identified by sample number. 'Terrestrial basalts' is an average value for basalts of the Earth. On the right, all laboratory data are terrestrial. Two curves for each rock type mark the typical lower and upper boundaries of velocities for such rock types.

breccias, and igneous rocks (Anderson *et al.*, 1970; Kanamori *et al.*, 1970, 1971; Wang *et al.*, 1971; and Warren *et al.*, 1971). Regardless of composition, these rocks are characterized by very low velocities at low pressures relative to terrestrial rocks. This can be attributed to the absence of water in the lunar rocks combined with the effects of porosity and micro-cracks. Laboratory measurements on terrestrial igneous rocks with about 0.5% porosity have demonstrated this effect as shown in Figure 9 (Nur and Simmons, 1969).

From the comparison of the laboratory data and the lunar velocity profile, the following units can be identified:

(i) Near the surface the extremely low seismic velocities (starting at 0.1 km/s are very similar to those of lunar fines (soils) and broken rocks. The velocity increases very rapidly as a result of self-compaction under pressure. The exact depth to the

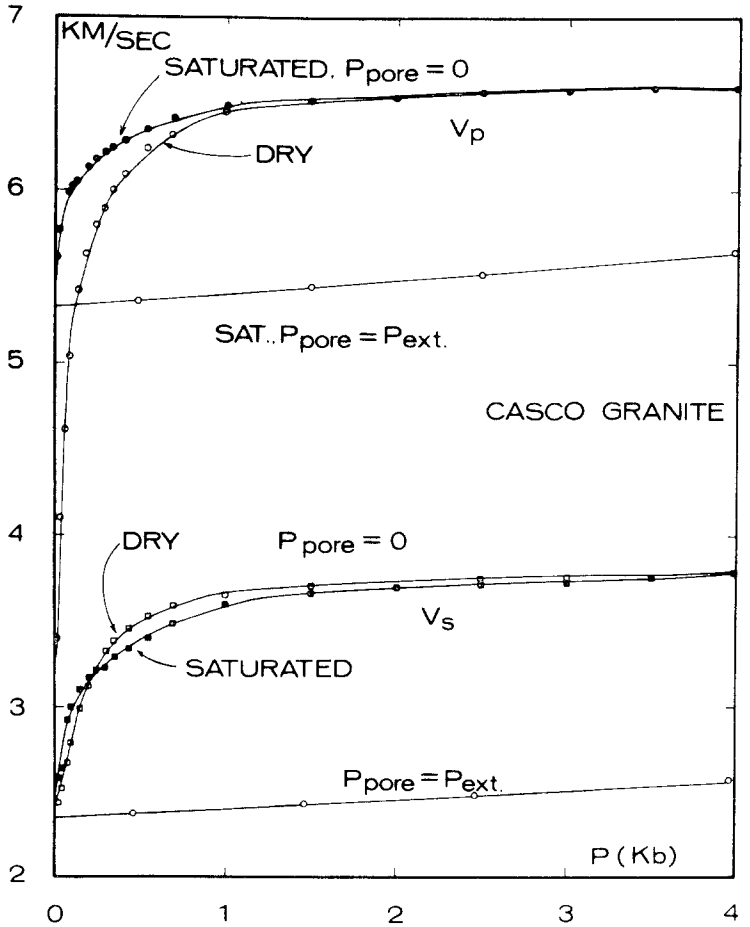

Fig. 9. Compressional and shear velocity versus pressure curves (laboratory data) for dry and water-saturated Casco granite (porosity = 0.7%). Note the large increase in P-wave velocity of the dry sample from 3.4 km/s at zero pressure to 6.4 km/s at one kilobar. This is analogous to lunar basalt samples shown in Figure 8 (after Nur and Simmons, 1971).

bottom of the lunar regolith and brecciated and fractured layer cannot be determined without additional travel-time data in the distance range of 0.1 to 5.0 km.

(ii) Below a depth of about 2 km the measured velocities of lunar basaltic rocks fit the velocity profile to a depth of about 25 km. The rapid increase of velocity to a depth of about 10 km can be explained by the pressure effect on dry rocks having micro- and macro-cracks. The observed velocity model seems to fall between the measured values for lunar rocks, Nos. 10057 and 12065, paralleling these curves to a depth of 25 km. Of the rocks shown on Figure 8, Nos. 12052, 12063, and 12065 are classified as Type 3 porphyritic basalts and No. 10057 as Type 2 intersertal basalt (Warner, 1971). Rock No. 12018 is Type 4 porphyritic basalt. Thus to a depth of about 25 km, the observed velocities are consistent with a basaltic composition. Whether this layer consists of a series of flows or fairly thick intrusive basalt cannot be resolved with our

data. Nor is it possible to rule out other compositions until velocity measurements are carried out on other lunar rock samples such as the anorthosite (sample No. 15415) returned by the Apollo 15 Mission.

(iii) At 25 km the velocity increases rapidly to a value of about 6.8 km/s. This marks the top of the second unit of the lunar crust. Although the exact details of the velocity increase cannot be specified with the available data, the velocity jump fits both the travel times and amplitudes better than smoother models. This layer extends to a depth of about 65 km with nearly constant velocity throughout (velocity at the bottom is about 7.0 km/s). The petrological interpretation of the velocity curve is not very simple. It is clear from Figure 8 that no returned lunar sample velocity fits the observed curve. Thus we must resort to laboratory data on terrestrial rocks (see Press, 1966; Anderson and Liebermann, 1966, for compilations). The examples plotted on Figure 8 represent some possible candidates. The observed velocity curve falls in the middle of the laboratory data for gabbros (including norite). It is also very close to the anorthosite values. The lower bound for terrestrial pyroxenite is slightly higher than the observed curve, but the difference is not large enough to exclude pyroxenite from consideration. Eclogite velocities are definitely higher than the observations and eclogite cannot be considered as a serious possibility.

To narrow the choice we must consider other data such as the density required to satisfy the mean density ($\bar{\varrho}=3.34$ g/cm^3) and the moment of inertia factor ($F=0.402$). Furthermore, a model consistent with the petrogenesis of lunar basalts, especially Apollo 12 basalts, must be sought (Green *et al.*, 1971; Biggar *et al.*, 1971; and Ringwood and Essene, 1970). When all data are considered, gabbro or an anorthositic gabbro composition is favored, although other interpretations are not ruled out.

(iv) The discontinuity at 65 km depth is required to satisfy the amplitudes, travel times, and most clearly the seismogram characteristics at $\Delta=357$ km. The velocities below this discontinuity increase to about 9 km/s. Although this velocity is based on a single point and is tentative until more seismic data becomes available from future impacts, the discontinuity is clearly a major structural boundary. It represents the lunar crust-mantle interface. The high velocities in the outer portion of the lunar mantle cannot be matched exactly with terrestrial values. A possible candidate whose velocity approaches the model velocity is Mg-rich olivine. Although not plotted, orthopyroxene-, and clinopyroxene-olivine rocks can also be accommodated and are favored from petrogenetic considerations (Ringwood and Essene, 1970; Green *et al.*, 1971). Spinel when added to the above could further raise the velocities. Whether the mantle is layered or relatively homogeneous in composition cannot be answered until additional seismic data extending to greater distances become available from future Apollo missions.

An additional point that must be clarified is the role that temperature might play in the interpretations. Thermal history calculations and temperature models indicate maximum temperatures of 300°C or less in the outer 100 km of the Moon (Toksőz *et al.*, 1972). The effect on velocities of such a temperature is less than 0.2 km/s and can be neglected.

4. Discussion and Conclusions

In the previous section we defined a lunar crust about 65 km thick for the southeast portion of Oceanus Procellarum. The crust consists of two major units and the base of the crust is defined with a major discontinuity. The upper layer, capped by regolith, brecciated and broken rocks, extends to a depth of 25 km. Whether this is compositionally homogeneous, primarily basaltic rock or represents a series of layers with different compositions but similar seismic velocities cannot be resolved. Rapid increase of velocities with depth in the upper 10 km is due to the closing of micro-cracks (intercrystalline and intergranular pores) and macro-cracks (structural cleavages and shock-induced cracks) under pressure. Heterogeneities and cracks combined with high velocity gradients and very low attenuation coefficients (high Q) due to very dry and vacuum-like conditions probably lead to extensive scattering of seismic waves. The increase of Q in dry rocks and in a vacuum has been demonstrated by laboratory measurements for both terrestrial (Pandit, 1971) and lunar (Warren *et al.*, 1971) rocks. The long and reverberating nature of lunar seismograms can be explained by such a scattering model (Latham *et al.*, 1970).

The composition of this first layer, if indeed it is primarily basaltic as indicated by the velocities, is in agreement with a model proposed by Wood (1970) on the basis of density contrast and relative elevations of basaltic mare and 'anorthositic' highlands. Isostatic compensation occurs for such a model if compositional differences extend to 25 km in depth – exactly the base of the first layer in our model. A thinner basalt layer covering and 'anorthosite' subbasement also must be considered as a possibility.

The second layer of the lunar crust (25 km to 65 km) appears to be made of competent rock. The increase in pressure affects velocities very little. Although a series of compositional alternatives are possible from matching velocities, the differentiation models favor norite, gabbro, or anorthositic gabbro instead of a felsic rock, such as pure anorthosite.

Upper mantle velocities exceeding 9 km/s are very high and caution must be exercised in the petrological interpretation until these velocities can be verified by additional data. Anisotropy of mantle rocks, structural trends and dipping interface problems could affect the apparent velocities. If this high velocity persists, then Mg-rich olivine, olivine with pyroxenes, or high pressure phases of crustal rocks should be considered as prime candidates. This implies a differentiated lunar mantle, with iron-rich olivines and pyroxenes remaining deeper in the mantle and acting as the source rock for lunar basalts such as Samples 12022 and 12065 (Green *et al.*, 1971). Although the mean density can be satisfied with such a model, the moment of inertia factor would require a density decrease still deeper in the lunar interior.

The above model implies the early differentiation and formation of a two-layer crust. The basalts which fill the low-lying areas and craters of the lunar surface represent differentiates from a partially molten lunar upper mantle at a later time. Based on the thermal calculations (Toksőz *et al.*, 1972, Figure 6) the crust mostly differentiated from the outer 400 km of the Moon within the first billion years of lunar

history. Partial melting below a depth of 200 km continued after this time and deep basalts could be generated from greater depths after the first billion years.

Acknowledgements

We are grateful to Drs. B. Julian, S. Solomon, and R. Wiggins for their help and contributions during many phases of this work. Our special thanks to Mr. E. Stolper for his relentless efforts and perseverence during the analysis and interpretation of the data. This research was supported by NASA, Grant No. NASA-NGR 72-009-123 at MIT, and by contract NAS 9-5957 at Lamont Doherty Geological Observatory.

References

Anderson, O. L. and Lieberman, R. C.: 1966, *VESIAC State of-the-Art Report*, No. 7885-4-X, Willow Run Laboratories, University of Michigan, p. 182.

Anderson, O. L., Scholz, C., Soga, N., Warren, N., and Schreiber, E.: 1970, *Proceedings of the Apollo 11 Lunar Science Conference* **3**, Pergamon Press, New York, p. 1959.

Biggar, G. M., O'Hara, M. J., and Peckett, A.: 1971, *Proceedings of the Second Lunar Science Conference* **1**, MIT Press, p. 617.

Green, D. H., Ringwood, A. E., Ware, N. G., Hibberson, W. O., Major, A., and Kiss, E.: 1971, *Proceedings of the Second Lunar Science Conference* **1**, MIT Press, p. 601.

Helmberger, D. V.: 1968, *Bull. Seism. Soc. Am.* **58**, 179.

Helmberger, D. V. and Wiggins, R. A.: 1971, *J. Geophys. Res.* **76**, 3229.

Kanamori, H., Nur, A., Chung, D. H., Wones, D., and Simmons, G.: 1970, *Science* **167**, 726.

Kanamori, H., Mizutani, H., and Yamano, Y.: 1971, *Proceedings of the Second Lunar Science Conference* **3**, The MIT Press, Cambridge, Massachusetts, p. 2323.

Kovach, R. L., Watkins, J. S., and Landers, T.: 1971, *Apollo 14 Preliminary Science Report*, NASA SP-272, p. 163.

Latham, G., Ewing, M., Dorman, J., Press, F., Toksőz, N., Sutton, G., Meissner, R., Duennebier, F., Nakamura, Y., Kovach, R., and Yates, M.: 1970, *Science* **170**, 620.

Latham, G., Ewing, M., Press, F., Sutton, G., Dorman, J., Nakamura, Y., Toksőz, N., Duennebier, F., Lammlein, D.: 1971a, *Apollo 14 Preliminary Science Report*, NASA SP-272, p. 133.

Latham, G., Ewing, M., Dorman, J., Lammlein, D., Press, F., Toksőz, N., Sutton, G., Duennebier, F., and Nakamura, Y.: 1971b, *Science* **174**, 687.

Nur, A. and Simmons, G.: 1969, *Earth Planetary Sci. Letters* **7**, 183.

Pandit, B. I.: 1971, 'Experimental Studies on the Mechanism of Internal Friction (Q^{-1}) of Rocks', Ph.D. Thesis, University of Toronto.

Press, F.: 1966, *Geol. Soc. Am. Mem.* **97**, 195.

Ringwood, A. E. and Essene, E.: 1970, *Proceedings of the Apollo 11 Lunar Science Conference* **1**, 769.

Toksőz, M. N., Solomon, S. C., Minear, J. W., and Johnston, D.: 1972, *The Moon* **4**, 190.

Wang, H., Todd, T., Weidner, D., and Simmons, G.: 1971, *Proceedings of the Second Lunar Science Conference* **3**, MIT Press, p. 2327.

Warner, J. L.: 1971, *Proceedings of the Second Lunar Science Conference* **1**, MIT Press, Cambridge, Mass., p. 469.

Warren, H., Schreiber, E., Scholz, C., Morrison, J. A., Norton, P. R., Kumazala, M., and Anderson, O. L.: 1971, *Proceedings of the Second Lunar Science Conference* **3**, MIT Press, Cambridge, Mass., p. 2345.

Wood, J. A.: 1970, *J. Geophys. Res.* **75**, 6497.